

Article

Flexural Strength and Acoustic Damage Characteristics of Steel Bar Reactive Powder Concrete

Tingyou Yi ^{1,2}, Hua Wang ^{3,4,*}, Juntao Xie ⁵ and Wensheng Wang ^{1,6,*} 

¹ Department of Road and Bridge, College of Transportation, Jilin University, Changchun 130025, China; dujw1717@mails.jlu.edu.cn

² Guangxi Beitou Highway Construction and Investment Group Co., Ltd., Nanning 530029, China

³ Guangxi Transportation Science and Technology Group Co., Ltd., Nanning 530007, China

⁴ Guangxi Beibu Gulf Investment Group Co., Ltd., Nanning 530029, China

⁵ Capital Construction Department, Guangxi Normal University, Guilin 541004, China; xingjj1717@mails.jlu.edu.cn

⁶ Department of Geological Engineering, College of Construction Engineering, Jilin University, Changchun 130025, China

* Correspondence: wanghua15@mails.jlu.edu.cn (H.W.); wangws@jlu.edu.cn (W.W.); Tel.: +86-0431-8509-5446 (W.W.)

Abstract: In this paper, the steel bar was used to prepare steel bar reactive powder concrete (SBRPC). The three-point bending test was adopted to investigate the effect of the number of steel bars on the flexural strength of SBRPC. The acoustic emission (AE) was used to monitor the fracture process of SBRPC in real time. In addition, the parameter RA and AF ratio (RF) was defined to analyze the distribution of shear cracks and tensile cracks during the fracture process. The experimental results showed that with the increases in the number of the steel bar, the flexural strength of SBRPC gradually increased. The fracture stage of SBRPC can be accurately divided according to the curve slope change in hits and cumulative counts. Moreover, the early warning of SBRPC damage can be realized by observing the amplitude of the AE amplitude value. The dynamic changes in the rising angle (RA) and average frequency (AF) values can be used to determine the cracks mode and fracture mode. Based on the results of RF analysis, adding steel bars will improve the proportion for tensile cracks during its fracture process.

Keywords: steel bar; reactive powder concrete; flexural strength; acoustic emission; fracture behavior



Citation: Yi, T.; Wang, H.; Xie, J.; Wang, W. Flexural Strength and Acoustic Damage Characteristics of Steel Bar Reactive Powder Concrete. *Appl. Sci.* **2021**, *11*, 7017. <https://doi.org/10.3390/app11157017>

Received: 14 June 2021

Accepted: 26 July 2021

Published: 29 July 2021

Publisher's Note: MDPI stays neutral with regard to jurisdictional claims in published maps and institutional affiliations.



Copyright: © 2021 by the authors. Licensee MDPI, Basel, Switzerland. This article is an open access article distributed under the terms and conditions of the Creative Commons Attribution (CC BY) license (<https://creativecommons.org/licenses/by/4.0/>).

1. Introduction

Reactive powder concrete (RPC), proposed in the 1990's [1], as a new type of ultra-high-performance concrete, has the characteristics of high strength, long service life, and good durability [2,3]. Therefore, it has become a cement-based material that is widely used and developed by the development of microstructure enhancement methods [4]. Its implementation methods include removing coarse aggregates, reducing water-binder ratio, optimizing particle classification, and adding silicon-containing active materials to increase the silica composition in the mixture [5,6]. In addition, the toughness of RPC can be improved by adding fibers [7]. Although the cost of RPC is relatively expensive, the purpose of saving materials and costs can be achieved by reducing the size of structural components [8]. However, RPC still has the mechanical characteristics of ordinary concrete [9]. The flexural strength of RPC is usually lower than its compressive strength. Therefore, adding steel bars in the concrete becomes a useful method to improve the flexural strength of RPC.

Some scholars have studied the interaction between RPC and steel bars. Al-Quraishi et al. [10] investigated the influences of the number of transverse steel bars on the tension splice intensity of steel bars embedded in RPC. The results showed that the tension splice strength increased with the number of steel bars. Alkaysi et al. [11] evaluated

the effect of the embedded depth of the steel bar on the bond intensity between the steel bar and RPC, and the peak bond intensity of specimens decreased with the increase in the embedded depth. Bae et al. [12] researched the bond stress between conventional steel bars and RPC. The experiment result showed that as the compressive strength of RPC increased, the bond stress gradually enhanced, but the corresponding increase rate gradually decreased. Nevertheless, relatively little research has been carried out for the fracture process of RPC reinforced with steel bars.

Acoustic emission (AE) technology, as a non-destructive method [13,14], is adopted to detect the real failure condition of structures, as well as material damage behavior [15]. It has the characteristics of high sensitivity, accurate location of damage sources, and real-time monitoring [16,17]. The internal damage of the concrete releases a certain intensity of elastic waves and propagates to the surface of the concrete [18,19], which are collected and processed by AE sensors into electrical signals and used for the fracture analysis for concrete [20]. At present, some scholars have studied the characteristics of concrete during the fracture damage process through AE technology. Bhosale et al. [21] researched the fracture behavior of concretes reinforced with synthetic fiber, steel fiber, as well as mixed fiber through AE technology, and divided the cracks as shear and tensile modes. Fan et al. [22] introduced AE technology into the study of uniaxial dynamic tension. The result showed that the increase rate of the AE parameters of concrete under dynamic load gradually decreased with the increase in the initial quasi-static load, and the more the initial loading period, the less the AE signal generated in the dynamic loading period. Rasheed et al. [23] adopted AE technology to study the fracture characteristics of concrete containing hybrid fiber, and they found that the identification of crack positions through AE analysis is pretty close to real fracture damage development.

In this paper, steel bar reactive powder concrete (SBRPC) was prepared with steel bars, and the influences of the steel bar number on flexural intensity and fracture behavior for SBRPC were investigated. The failure process of SBRPC was evaluated based on the AE parameter direct analysis method, and the failure mode of SBRPC was investigated through the AE indirect calculation analysis method. In addition, the distribution of the shear cracks and tensile cracks of SBRPC was investigated through the defined parameter.

2. Materials and Methods

2.1. Materials

The cementitious material used Portland cement of P.O 42.5 MPa and the corresponding properties index are shown in Table 1. The silica fume (SF93) was adopted as active material in this study, its specific surface area is 18,100 m²/kg. The chemical components of SF93 silica fume and P.O 42.5 MPa cement are listed in Figure 1. Three types of quartz sand (20–40, 40–80, and 80–120 mesh) were used as aggregate. The quartz powder with 400 mesh was used as fill materials. Table 2 shows the chemical components of quartz sand. HPWR-Q8011 superplasticizer was used to improve concrete workability, for which the water reduction rate was about 25%. The properties of chopped basalt fiber, as a reinforcement material, are presented in the previous study [24]. Type HPB300 rebar (diameter: 8 mm, length 380 mm) was used for concretes, the tensile strength of rebar was 445 MPa, and its yield strength was 335 MPa. The elastic modulus of the rebar was 2.1×10^5 MPa. The tap water was used as mixed water.

Table 1. The performance index of cement.

Density (kg/m ³)	Specific Surface Area (m ² /kg)	Setting Time (min)		Compressive Strength (MPa)	Flexural Strength (MPa)
		Initial Setting	Final Setting		
3160	385	91	145	62.2	9.1

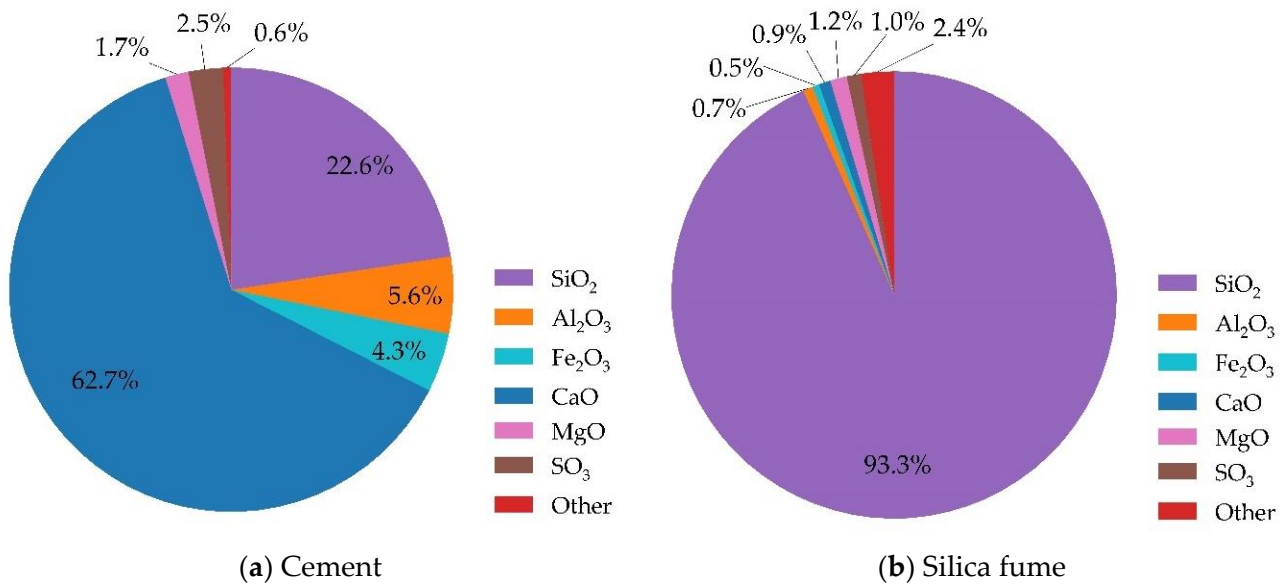


Figure 1. The chemical components of cement and silica fume: (a) P.O 42.5 MPa cement, (b) SF93 silica fume.

Table 2. The composition of quartz sand.

Material	Chemical Components (%)					
	SiO ₂	Fe	Al ₂ O ₃	K ₂ O	Na ₂ O	H ₂ O
Quartz Sand	99.68	0.0062	0.0122	0.0011	0.002	0.02

2.2. Preparation of SBRPC

In this paper, the steel bar and RPC were combined to prepare an SBRPC specimen with the size of 400 mm × 100 mm × 100 mm, where its mixture proportion of RPC is given in Table 3. The 400-mesh sandpaper was adopted to polish the steel bar until metallic luster appeared.

Table 3. The mixture proportion of reactive powder concrete (RPC) (kg/m³).

Mix	Quartz Sand	Cement	Silica Fume	Quartz Powder	Basalt Fiber	Water	Water Reducer
RPC	947.0	841.8	210.4	311.4	12	151.5	52.6

The ISO 679 mixer was adopted to prepare the RPC mixer. Before pouring RPC, the steel bars were laid up at the bottom of the mold, the number of those placed was one, three, and five, and the molded specimens were marked as SBRPC-1, SBRPC-3, and SBRPC-5. The placement of the steel bars is shown in Figure 2. The specimen after standing for 24 h was cured for 48 h in an environment of 90 °C. The flexural strength of SBRPC was evaluated and its corresponding failure process of specimens was monitored through AE technology.

2.3. Flexural Strength Test

In this paper, the flexural strength of SBRPC was tested according to national standard GB/T50081-2002 [25]. The flexural strength experimental method for SBRPC was a three-point bending test using the universal testing machine. The calculated span (fulcrum distance) of SBRPC is 300 mm. While conducting the flexural test, the flexural failure and damage crack of SBRPC were monitored based on AE technology. The specific test schematic diagram is shown in Figure 3.

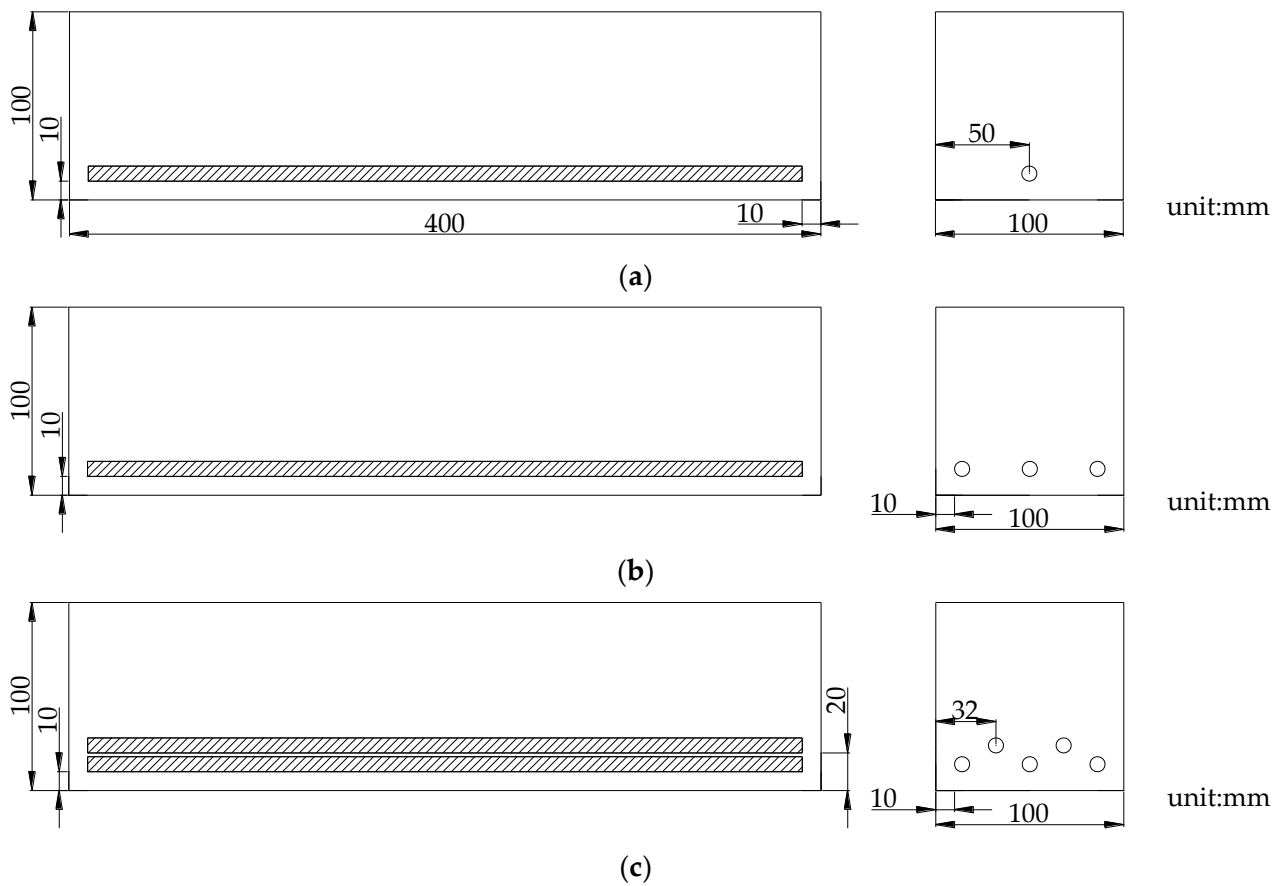


Figure 2. Schematic diagram of the steel bar reactive powder concrete (SBRPC): (a) SBRPC-1; (b) SBRPC-3; (c) SBRPC-5.

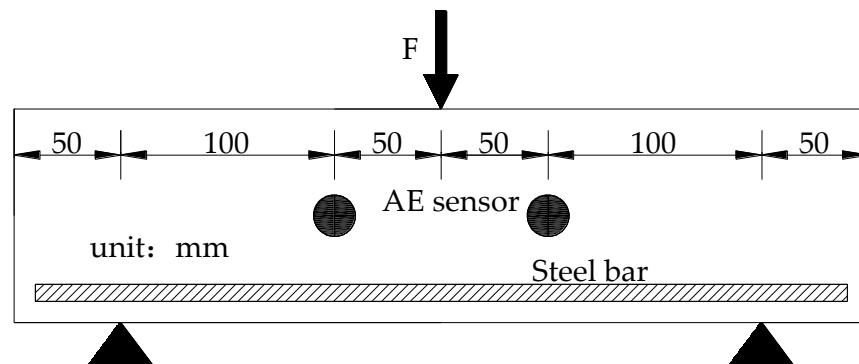


Figure 3. Schematic diagram of flexural strength test.

2.4. AE Test

AE technology could detect the initiation and expansion of SBRPC cracks through a non-destructive method, and at the same time could judge the damage mode of SBRPC. In general, the acoustic properties of SBRPC could be studied by using the direct parameter analysis and indirect calculation analysis. The direct parameters of AE technology include amplitude, rise time, energy, duration, and counts. The descriptions of acoustic emission signals are plotted in Figure 4. Amplitude refers to the maximum amplitude value of the AE signal. Rise time refers to the time interval from the first time the AE signal amplitude exceeds the threshold to the maximum value. Energy refers to the elastic energy released by an AE event. Duration refers to the time interval between when the event signal first exceeds the threshold and finally falls below the threshold. Count refers to the number of AE amplitudes that exceed the threshold [26,27].

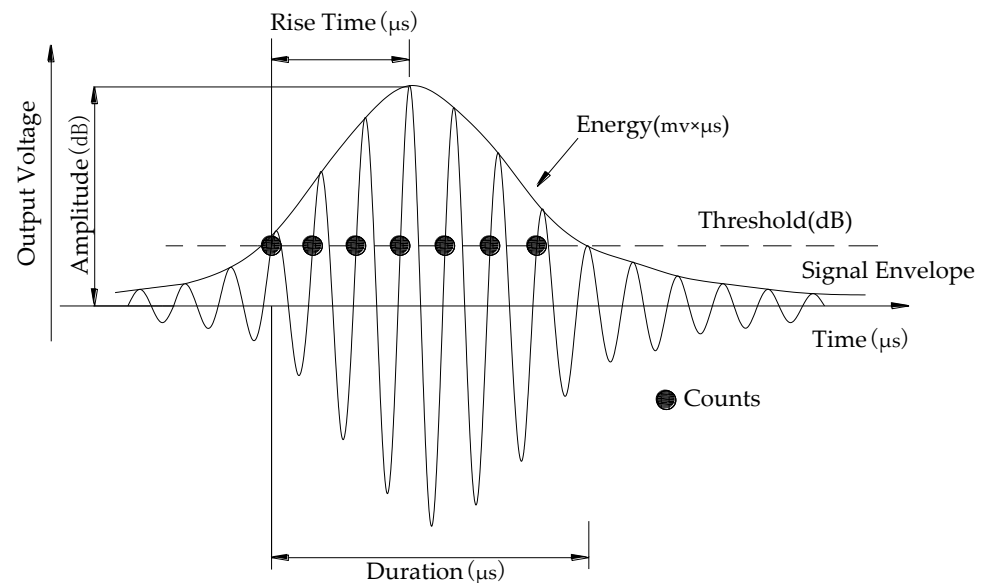


Figure 4. Schematic diagram of acoustic emission (AE) parameters.

Commonly used indirect calculation analysis of AE technology is rise angle (RA)/average frequency (AF) and used to classify failure and its mode [28], their calculation formulas of AF and RA are as follows:

$$AF = \frac{\text{Counts}}{\text{Duration}}, \text{kHz} \quad (1)$$

$$RA = \frac{\text{Rise time}}{\text{Amplitude}}, \text{ms/V} \quad (2)$$

$$\text{dB} = 20 \lg \frac{V}{V_{\text{ref}}}; V_{\text{ref}} = 10^{-6} \text{ V} = 0 \text{ dB} \quad (3)$$

There are two types of failure modes of SBRPC, namely, tensile (smaller RA and larger AF) and shear (larger RA and smaller AF) modes.

The fracture development of SBRPC was real-time monitored by the AE acquisition and analysis system. The SR150M 150 kHz resonant AE sensors were symmetrically arranged at both sides of the loading point, its specific arrangement is shown in Figure 3. Before the test, AE sensors were tested to make sure they were in good condition by lead-breaking test in advance. The threshold of the acquisition system was set to 40 dB. The specific AE acquisition parameters are detailed in the existing literature [29].

3. Results and Discussion

3.1. Flexural Strength

The flexural strength of SBRPC was tested to analyze the influence of steel bars on the bending resistance of SBRPC. Figure 5 plots the changing trend of the flexural strength of the SBRPC specimen as steel bar number.

Figure 5 implies that the flexural strength of SBRPC increases with the increase in the number of steel bars. In the mechanical test, the upper surface of SBRPC was compressed and the lower surface was tensioned. RPC has excellent compressive strength, but its resistance to tensile strength is not as good as its excellent compressive strength. The steel bar shows excellent tensile properties. The cooperation of steel bars and RPC can effectively improve the performance of SBRPC against bending stress. Figure 5 shows that the flexural strength of SBRPC increases with the increase in the number of steel bars. When the number of steel bars is less than three, the flexural strength of SBRPC is smaller than that of SBPPC-3 and SBRPC-5, which indicates that a small number of steel bars could not increase the SBRPC strength, obviously, and an appropriate and excessive amount of steel bars can effectively improve its flexural strength. The failure state of the SBRPC is

shown in Figure 6. It can be seen from Figure 6 that when the specimen is damaged, the concrete at the stress point is broken and the steel bar is bent.

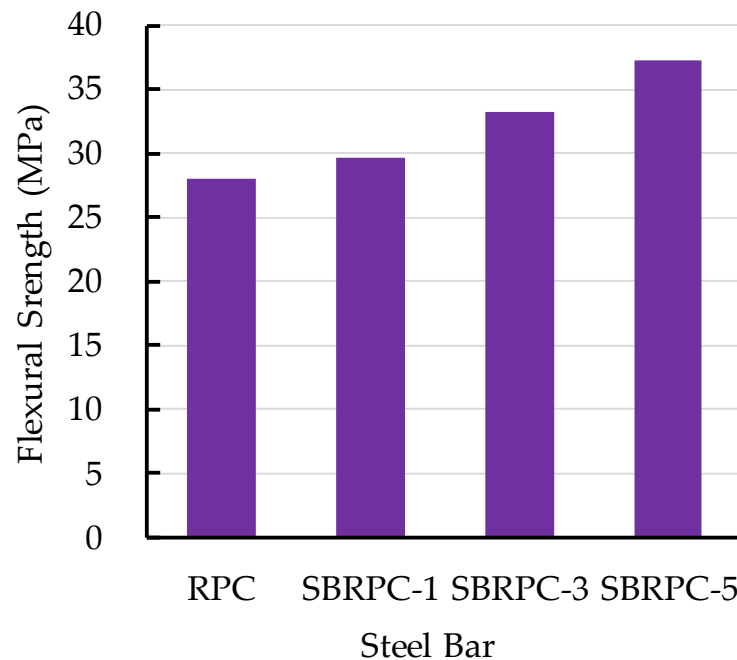


Figure 5. The effect of a steel bar on the flexural strength of SBRPC.



Figure 6. The failure state of SBRPC.

3.2. AE Parameters Direct Analysis

In this paper, two AE sensors were adopted in order to monitor the failure process of SBRPC. In the following figure, Figure 1 was the signal collected by the sensor on the left side of the load point, and Figure 2 was the signal collected by the sensor on the right. The load level is defined as the load at some point divided by the maximum load.

3.2.1. Hits and Counts

Figure 7 shows the curve of the AE signal that was collected during the failure of the SBRPC. The damage process could be delimited as four periods, considering the slope changes in hits and cumulative counts curves. The hits and cumulative counts increased quickly in stage II, which could be attributed to a large number of micro-cracks that appeared in this stage. In stage III, the above-mentioned cracks are connected and penetrated, and, finally, the specimen enters stage IV, thereby being destroyed. However, the critical diacritical point in the failure specimen period is different based on visually analyzing the AE parameters collected by the two sensors, which shows that there is a

difference in the failure process of the loading symmetrical parts, and the right part beside the loading point has a faster failure process. The combination of steel bars and RPC can effectively improve the SBRPC failure resistance. From Figure 7b–d, the critical diacritical point of SBRPC failure appears under the same loading degree, which is related to the joint action of steel bars and RPC. The damage process of SBRPC can be delimited into three periods, considering the slope changes in hits and cumulative counts curves. Compared with RPC, the duration of stage I of SBRPC is longer, which shows that the steel bars can effectively bear part of the load and inhibit the generation of micro-cracks during the loading process. In addition, compared with SBRPC-3, the hits and cumulative counts of SBRPC-1 and SBRPC-5 undergo a significant abrupt change, which is related to the number of steel bars. The appropriate number of steel bars is more beneficial to the force form of SBRPC.

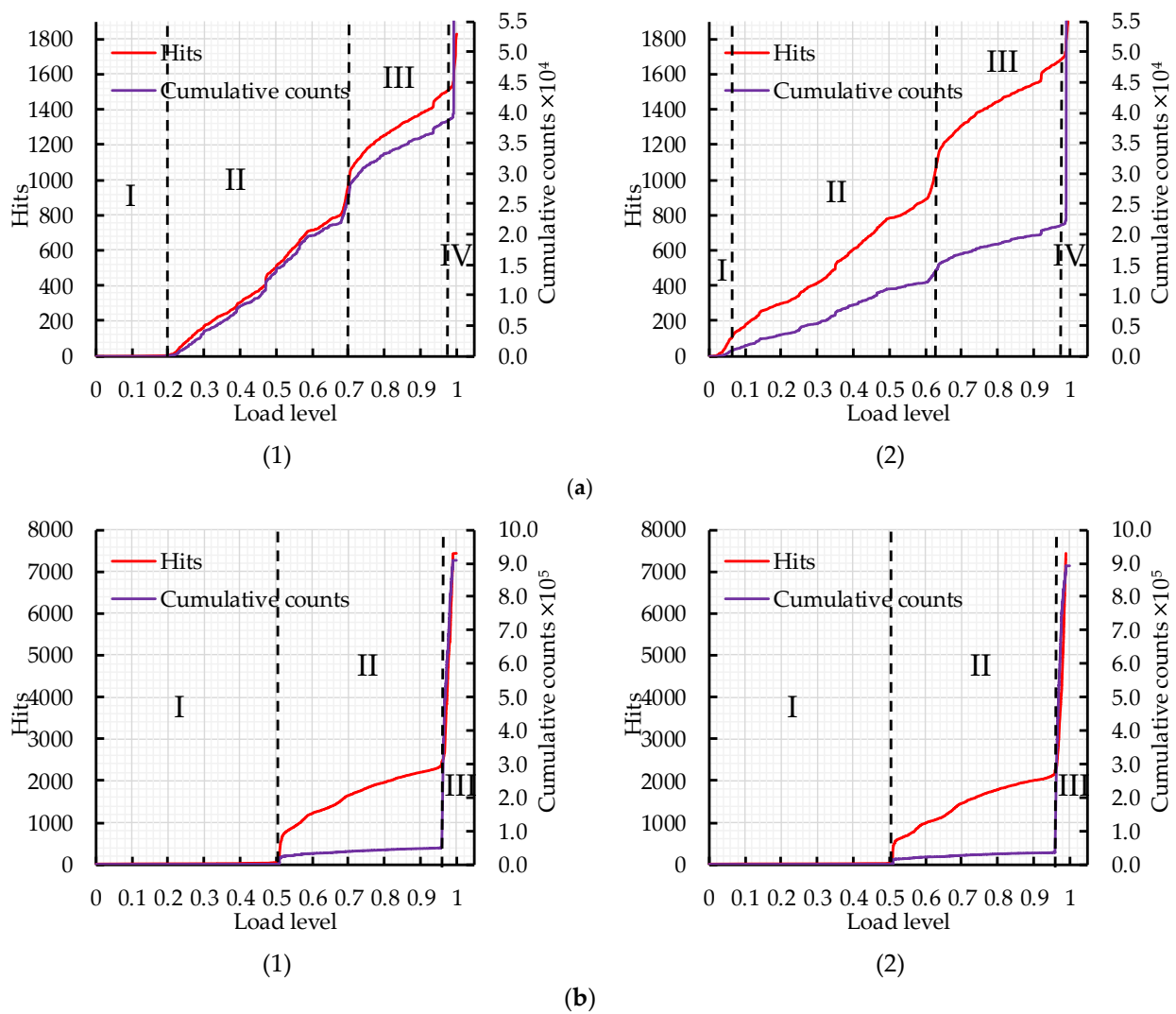


Figure 7. Cont.

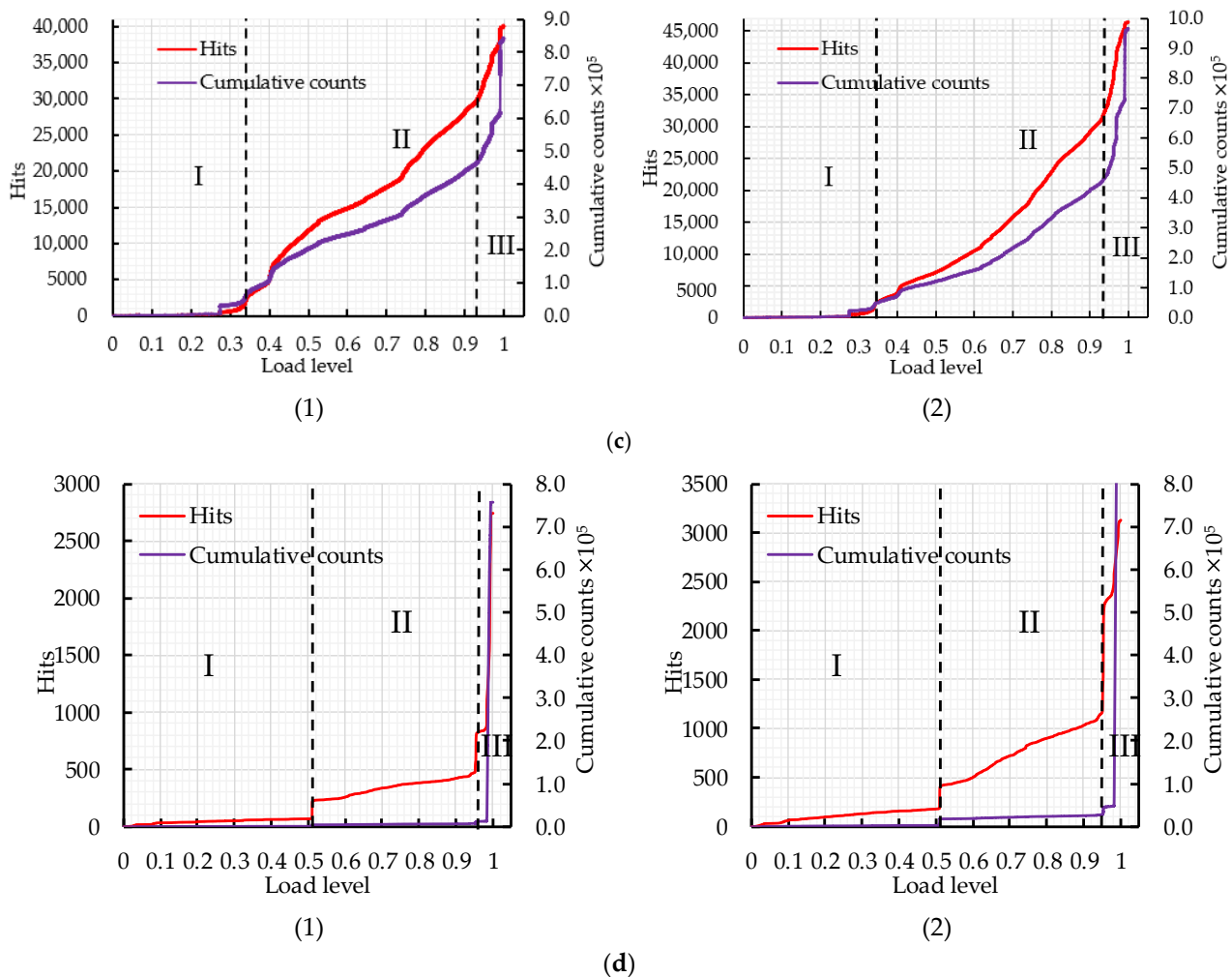


Figure 7. The variation curve of hits and cumulative counts: (a) RPC; (b) SBRPC-1; (c) SBRPC-3; (d) SBRPC-5.

3.2.2. Amplitude

The distribution of AE amplitude values is summarized in Figure 8, and it is also divided based on the hits and cumulative counts. Figure 8 shows that the amplitude values show an overall increasing trend with the loading degree, which has some links with the damage degree of the specimens. As the failure progresses, more and more micro-cracks sprout and develop into macro-cracks, releasing high-strength elastic waves, thereby forming high-amplitude value AE signals. Figure 8a presents that most of the amplitude signal appears in stages II and III, and the values are between 40 dB and 60 dB. When the SBRPC specimen enters the failure stage, the AE reaches above 70 dB. Figure 8b shows that the AE amplitude signal in stage I is less, which indicates that few internal micro-cracks occur inside the specimen. The amplitude values could reach 50 dB when entering stage II, and the signal value abruptly increases again around 70 dB, indicating that the SBRPC specimen appears macroscopically damaged. In Figure 8c, the AE amplitude value shows an increasing trend as the load level increases. The maximum signal value achieves 50 dB in stage I, 70 dB in stage II, and 80 dB in stage III. At the final, the signal value would reach up to 90 dB when the specimen breaks. Figure 8d plots that the signal value suddenly increases when entering stages II and III, which shows that a sudden change in the signal value could be adopted, to judge the transition of the specimen failure stage.

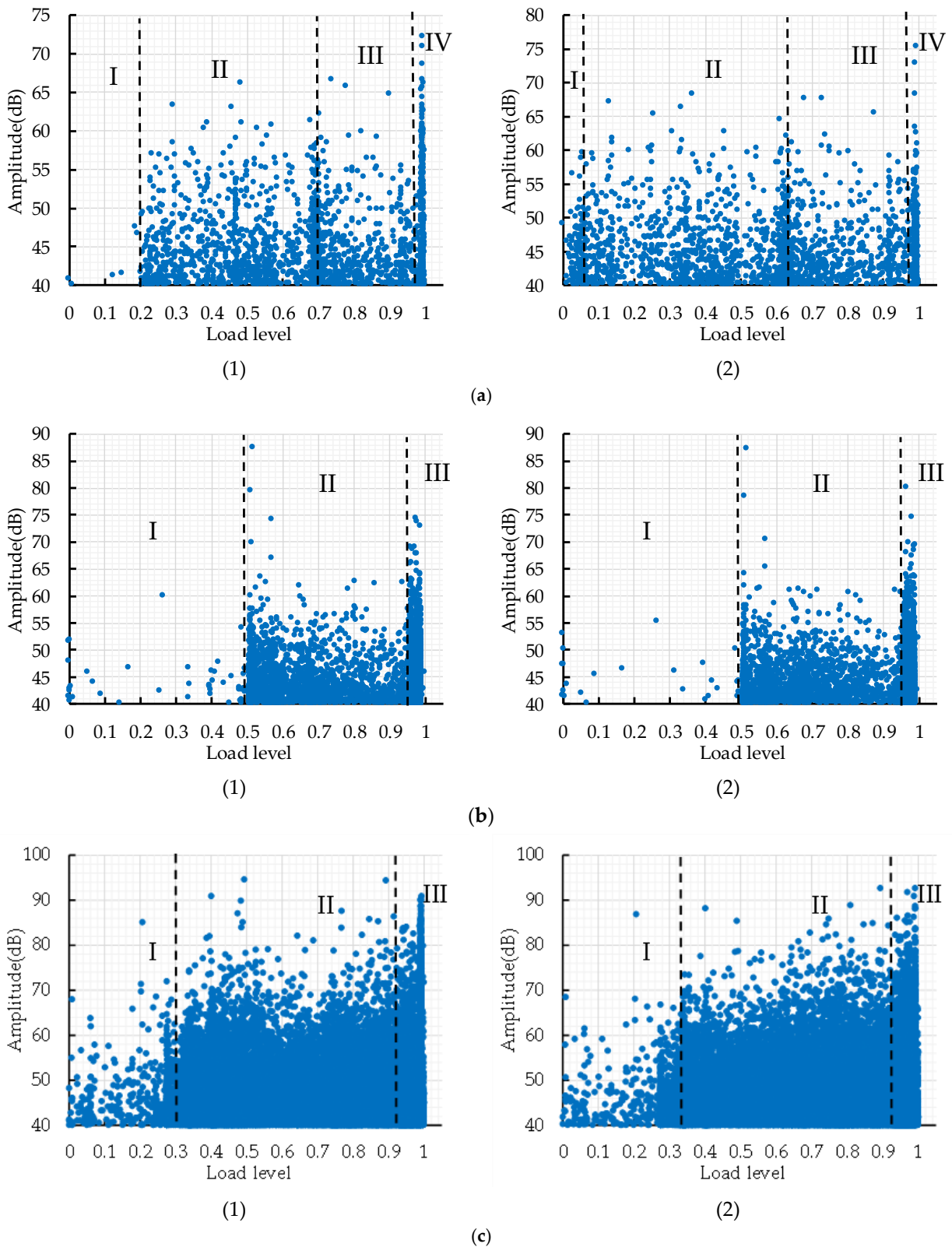


Figure 8. Cont.

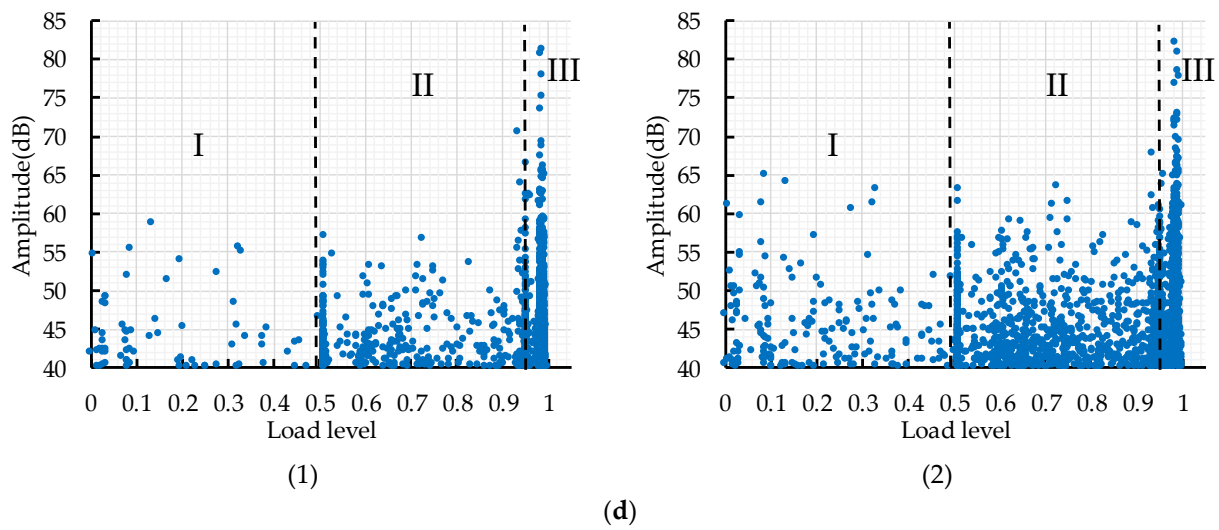


Figure 8. The distribution of AE amplitude: (a) RPC; (b) SBRPC-1; (c) SBRPC-3; (d) SBRPC-5.

3.3. AE Indirect Caculation Analysis

Figure 9 shows the RA and AF curves during the SBRPC failure. The RA, as well as AF, magnitudes change dynamically, implying the transformation for failure types of SBRPC. During the specimen failure process, the order for cracks initiation in the concrete matrix is considered to start from tensile cracks, and the shear cracks are gradually active as the cracks expand and fiber drawing events occur [30,31]. Figure 8 shows that the specimen in the failure stage would have larger RA values or smaller AF values with respect to the initial ones, indicating that when the SBRPC specimen is damaged, the shear mode is in an important position. In the period of crack development, RA and AF are in a dynamic fluctuation condition, and this indicates tensile cracks and shear cracks coexist at this stage. It can be seen from Figure 9a,b that RPC and SBRPC-1 have a lower initial RA value or a higher initial AF value, so there will be more shear cracks in the process of specimen failure or shear cracks dominate the failure of the specimen. As shown in Figure 9c,d, SBRPC-3 and SBRPC-5 have a larger initial RA or a smaller initial AF. Therefore, compared with RPC and SBRPC-1, there will be more tensile cracks in the process, implying a combined effect of steel bars and RPC could affect the failure mode of the specimen.

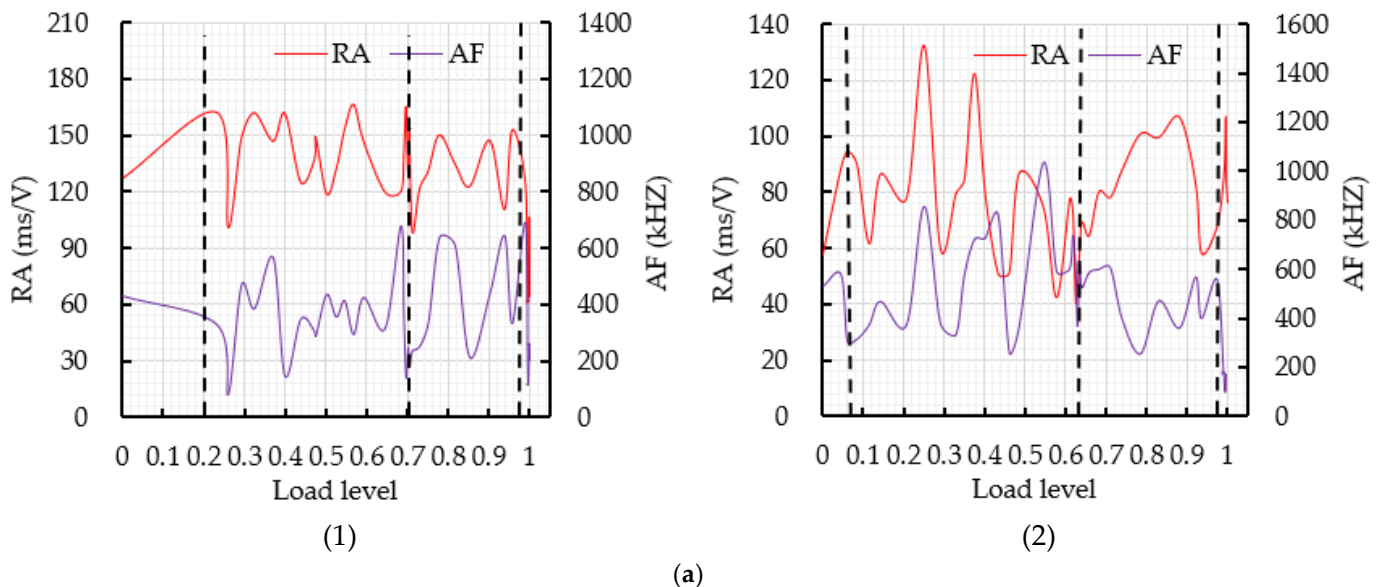


Figure 9. Cont.

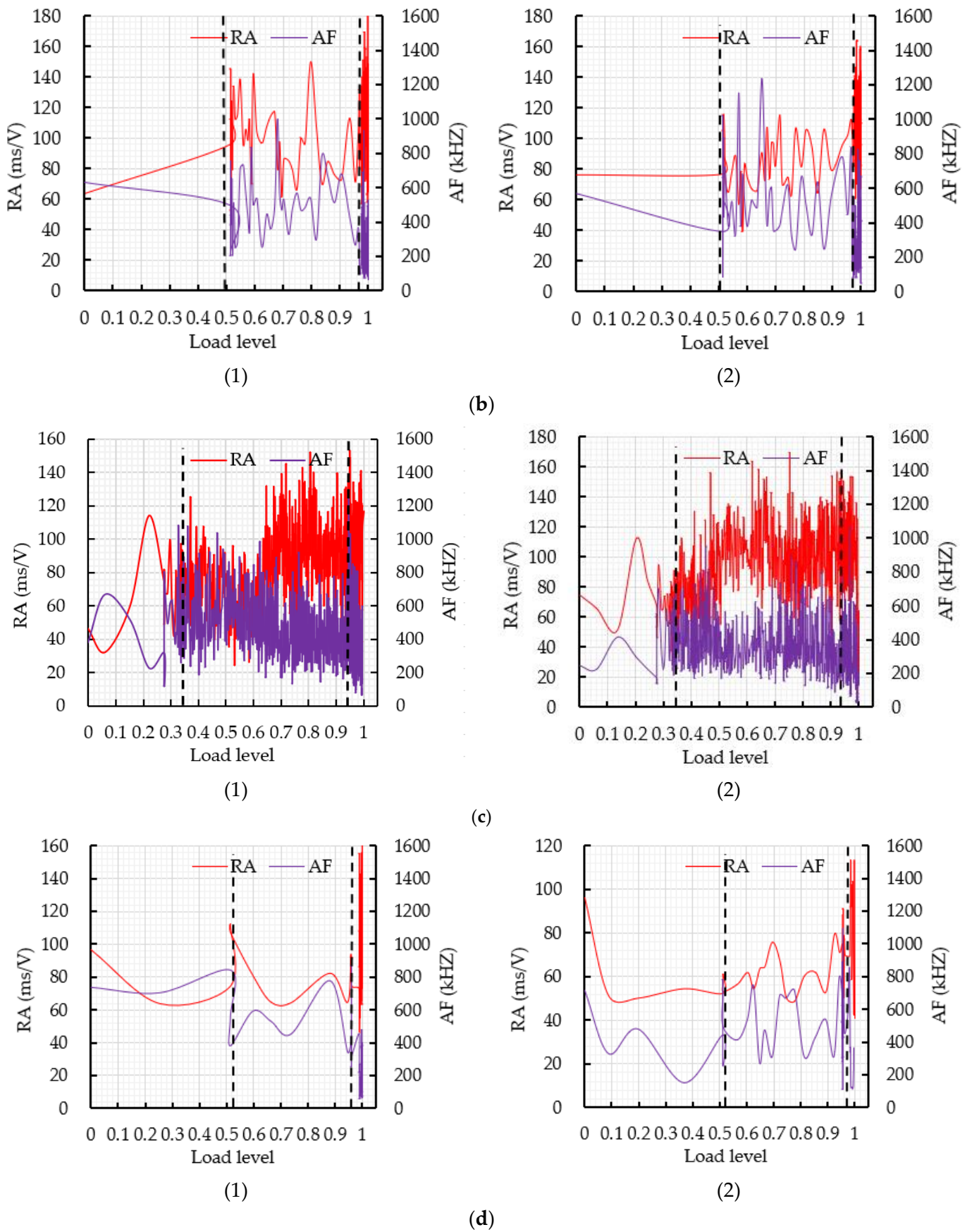


Figure 9. The variation curve of RA and AF: (a) RPC; (b) SBRPC-1; (c) SBRPC-3; (d) SBRPC-5.

To clearly characterize the transformation of the crack mode of the SBRPC during the fracture process, a parameter RA and AF ratio (RF) is defined in this paper. The calculation formula of RF is as follows:

$$RF = \frac{RA}{RA_{initial}} - \frac{AF}{AF_{initial}} \tag{4}$$

The variation curve of the load level and defined parameter RF is plotted in Figure 10. Figure 10a,b implies that the main crack mode to the specimen during the failure process is shear cracks, accounting for more than 80% of the crack amount. This is related to the RPC failure mode, and the pulling and friction events of the fiber cause the shear mode to be more active. Figure 10c,d indicates that during the concrete matrix failure on its right side of the loading point of SBRPC-3 and SBRPC-5, more tensile cracks occurred compared with RPC and SBRPC-1. This is related to the combination of steel bars and RPC; the RPC near the steel bars undergoes tensile failure along with the tensile strain of the steel bars.

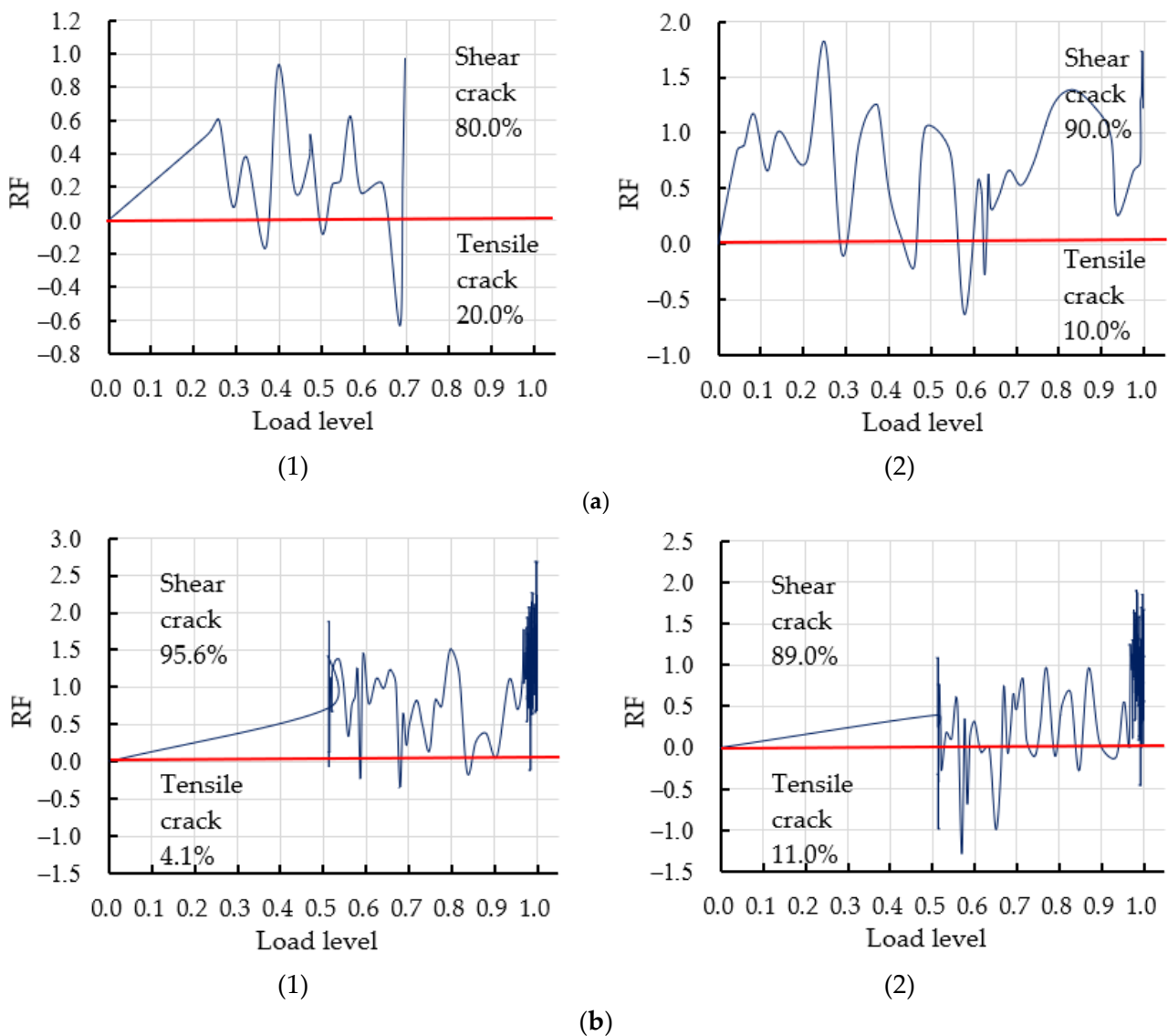


Figure 10. Cont.

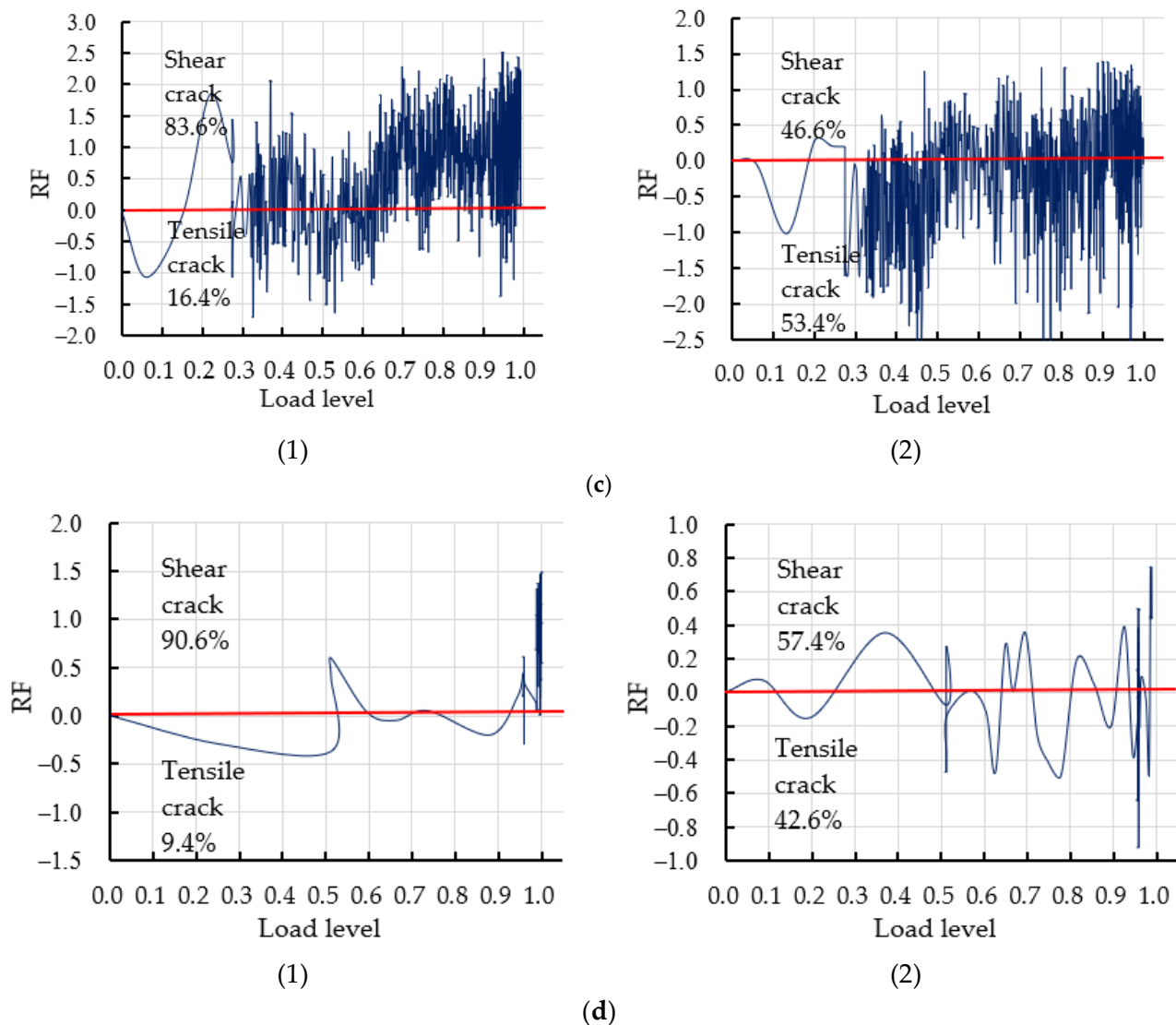


Figure 10. The variation curve of RF: (a) RPC; (b) SBRPC-1; (c) SBRPC-3; (d) SBRPC-5.

4. Conclusions

In this paper, the steel bar was adopted to prepare SBRPC, and the effect of the number of steel bars on the flexural strength of SBRPC was assessed. Simultaneously, the failure of the SBRPC specimen was real-time monitored by AE technology during its three-point bending test. The AE parameters direct and indirect analysis methods were adopted to investigate the fracture process and failure mode for SBRPC.

- (1) The flexural strength of SBRPC improves as the steel bar number increases. The flexural strength of SBRPC-5 is 37.32 MPa, which is 33.2% higher than that of RPC. The cooperation of steel bars and RPC can effectively improve the performance of RPC against bending stress;
- (2) The AE parameters can be used to describe the failure procedures of SBRPC. The failure stage of SBRPC could be delimited accurately, considering hits and cumulative counts;
- (3) AE amplitude will suddenly change at the critical diacritical point in the failure period, which indicates that AE amplitude could be applied for an early warning of damage;
- (4) The addition of steel bars would affect the distributions for shear and tensile cracks in SBRPC. In addition, the damage mode of the structure could be judged through RA, AF and RF, which provide a reference for practical engineering applications;

- (5) The acoustic damage characteristics of a fully reinforced RPC beam will be investigated in future studies.

Author Contributions: Conceptualization, H.W. and W.W.; methodology, H.W. and W.W.; validation, J.X.; formal analysis, T.Y., W.W.; investigation, T.Y. and J.X.; writing—original draft preparation, W.W.; writing—review and editing, and H.W.; project administration, H.W. and W.W.; funding acquisition, H.W. and W.W. All authors have read and agreed to the published version of the manuscript.

Funding: This research was supported by China Postdoctoral Science Foundation (grant number: 2021T140262). This research was also funded by Nanning Excellent Young Scientist Program (grant number: RC20180108), Nanning Excellent Young Scientist Program and Guangxi Beibu Gulf Economic Zone Major Talent Program (grant number: RC20190206), Science & Technology Base & Talent Special Project of Guangxi Province (grant number: AD19245152), “Yongjiang plan” of Nanning leading talents in innovation and Entrepreneurship (grant number: 2018-01-04).

Institutional Review Board Statement: Not applicable.

Informed Consent Statement: Not applicable.

Data Availability Statement: The data presented in this study are available on request from the corresponding author.

Acknowledgments: The authors would like to appreciate anonymous reviewers for their constructive suggestions and comments to improve the quality of the paper. Thanks to Wenjun Li for technical support in the testing procedure and data processing.

Conflicts of Interest: The authors declare no conflict of interest.

References

- Richard, R.; Cheyrezy, M. Composition of reactive powder concrete. *Cem. Concr. Res.* **1995**, *25*, 1501–1511. [\[CrossRef\]](#)
- Zhang, Y.S.; Sun, W.; Liu, S.F.; Jiao, C.J.; Lai, J.Z. Preparation of C200 green reactive powder concrete and its static-dynamic behaviors. *Cem. Concr. Comp.* **2008**, *30*, 831–838.
- Yazıcı, H.; Yardımcı, M.Y.; Aydın, S.; Karabulut, A.S. Mechanical properties of reactive powder concrete containing mineral admixtures under different curing regimes. *Constr. Build. Mater.* **2009**, *23*, 1223–1231. [\[CrossRef\]](#)
- Chan, Y.W.; Chu, S.H. Effect of silica fume on steel fiber bond characteristics in reactive powder concrete. *Cem. Concr. Res.* **2004**, *34*, 1167–1172. [\[CrossRef\]](#)
- Mostofinejad, D.; Nikoo, M.R.; Hosseini, S.A. Determination of optimized mix design and curing conditions of reactive powder concrete (RPC). *Constr. Build. Mater.* **2016**, *123*, 754–767. [\[CrossRef\]](#)
- Wille, K.; Boisvert-Cotulio, C. Material efficiency in the design of ultra-high performance concrete. *Constr. Build. Mater.* **2015**, *86*, 33–43. [\[CrossRef\]](#)
- Afrouhsabet, V.; Biolzi, L.; Ozbakkaloglu, T. High-performance fiber-reinforced concrete: A review. *J. Mater. Sci.* **2016**, *51*, 6517–6551. [\[CrossRef\]](#)
- Yazıcı, H.; Yardımcı, M.Y.; Yigiter, H.; Aydın, S.; Türkel, S. Mechanical properties of reactive powder concrete containing high volumes. *Cem. Concr. Comp.* **2010**, *32*, 639–648. [\[CrossRef\]](#)
- Ple, O.; Bayard, O. Preliminary study of multiscale analysis in fibre reinforced concrete. *Mater. Struct.* **2002**, *35*, 279–284. [\[CrossRef\]](#)
- Al-Quraishi, H.; Al-Farttoosi, M.; Abdul Khdhur, R. Tensile lap splice length of reinforcing bars embedded in reactive powder concrete (RPC). *Structures* **2019**, *19*, 362–368. [\[CrossRef\]](#)
- Alkaysi, M.; EL-Tawil, S. Factors affecting bond development between ultra high performance concrete (UHPC) and steel bar reinforcement. *Constr. Build. Mater.* **2017**, *144*, 412–422. [\[CrossRef\]](#)
- Bae, B.; Choi, H.K.; Choi, C.S. Bond stress between conventional reinforcement and steel fibre reinforced reactive powder concrete. *Constr. Build. Mater.* **2016**, *112*, 825–835. [\[CrossRef\]](#)
- Xie, C.; Yuan, L.J.; Zhao, M.; Jia, Y.H. Study on failure mechanism of porous concrete based on acoustic emission and discrete element method. *Constr. Build. Mater.* **2020**, *235*, 117409. [\[CrossRef\]](#)
- Carpinteri, A.; Xu, J.; Lacidogna, G.; Manuello, A. Reliable onset time determination and source location of acoustic emission in concrete structures. *Cem. Concr. Comp.* **2012**, *34*, 529–537. [\[CrossRef\]](#)
- Han, Q.H.; Yang, G.; Xu, J.; Fu, Z.W.; Lacidogna, G.; Carpinteri, A. Acoustic emission data analyses based on crumb rubber concrete beam bending tests. *Eng. Fract. Mech.* **2019**, *210*, 189–202. [\[CrossRef\]](#)
- Rouchier, S.; Foray, G.; Godin, N.; Woloszyn, M.; Roux, J.J. Damage monitoring in fibre reinforced mortar by combined digital image correlation and acoustic emission. *Constr. Build. Mater.* **2013**, *38*, 371–380. [\[CrossRef\]](#)
- Nair, A.; Cai, C.S. Acoustic emission monitoring of bridges: Review and case studies. *Eng. Struct.* **2010**, *32*, 1704–1714. [\[CrossRef\]](#)

18. Tsangouri, E.; Aggelis, D.G. A review of acoustic emission as indicator of reinforcement effectiveness in concrete and cementitious composites. *Constr. Build. Mater.* **2019**, *224*, 198–205. [[CrossRef](#)]
19. Sagar, R.V.; Prasad, B.K.R. A review of recent developments in parametric based acoustic emission techniques applied to concrete structures. *Nondestruct. Test. Eval.* **2012**, *27*, 47–68. [[CrossRef](#)]
20. Xu, J.; Fu, Z.W.; Han, Q.H.; Lacidogna, G.; Carpinteri, A. Micro-cracking monitoring and fracture evaluation for crumb rubber concrete based on acoustic emission techniques. *Struct. Health Monit.* **2018**, *17*, 946–958. [[CrossRef](#)]
21. Bhosale, A.; Rasheed, M.A.; Prakash, S.S.; Raju, G. A study on the efficiency of steel vs. synthetic vs. hybrid fibers on fracture behavior of concrete on flexure using acoustic emission. *Constr. Build. Mater.* **2019**, *199*, 256–268. [[CrossRef](#)]
22. Fan, X.Q.; Hu, S.W.; Lu, J.; Wei, C.J. Acoustic emission properties of concrete on dynamic tensile test. *Constr. Build. Mater.* **2016**, *114*, 66–75.
23. Rasheed, M.A.; Prakash, S.S.; Raju, G.; Kawasaki, Y. Fracture studies on synthetic fiber reinforced cellular concrete using acoustic emission technique. *Constr. Build. Mater.* **2018**, *169*, 100–112. [[CrossRef](#)]
24. Liu, H.; Lyu, X.; Zhang, Y.; Luo, G.; Li, W. Steel corrosion evaluation of basalt fiber RPC affected by crack and steel-concrete interface damage using electrochemical methods. *Sensors* **2020**, *20*, 5027. [[CrossRef](#)] [[PubMed](#)]
25. Ministry of Housing and Urban-Rural Construction of the People's Republic of China. *Standard for Test Method of Mechanical Properties on Ordinary Concrete*; Ministry of Housing and Urban-Ural Construction of the People's Republic of China: Beijing, China, 2002. (In Chinese)
26. Liang, C.; Ma, J.; Zhou, P.; Ma, G.; Xu, X. Fracture damage properties of SBS-modified asphalt mixtures reinforced with basalt fiber after freeze-thaw cycles using the acoustic emission approach. *Appl. Sci.* **2020**, *10*, 3301. [[CrossRef](#)]
27. Tan, G.J.; Zhu, Z.Q.; Wang, W.S.; Wu, C.L.; Ou, J.; Cui, G.J.; Zhang, D.M. Flexural ductility and crack-controlling capacity of polypropylene fiber reinforced ecc thin sheet with waste superfine river sand based on acoustic emission analysis. *Constr. Build. Mater.* **2021**, *277*, 122321. [[CrossRef](#)]
28. Ohtsu, M. Recommendations of RILEM Technical Committee 212-ACD: Acoustic emission and related NDE techniques for crack detection and damage evaluation in concrete: 3. Test method for classification of active cracks in concrete structures by acoustic emission. *Mater. Struct.* **2010**, *43*, 1187–1189.
29. Jiao, Y.B.; Fu, L.X.; Shan, W.C.; Liu, S.Q. Damage fracture characterization of pervious asphalt considering temperature effect based on acoustic emission parameters. *Eng. Fract. Mech.* **2019**, *210*, 147–159. [[CrossRef](#)]
30. Aggelis, D.G.; Soulitoti, D.V.; Sapouridis, N.; Barkoula, N.M.; Paipetis, A.S.; Marikas, T.E. Acoustic emission characterization of the fracture process in fibre reinforced concrete. *Constr. Build. Mater.* **2011**, *25*, 4126–4131. [[CrossRef](#)]
31. Soulioti, D.; Barkoula, N.M.; Paipetis, A.; Matikas, T.E.; Shiotani, T.; Aggelis, D.G. Acoustic emission behavior of steel fibre reinforced concrete under bending. *Constr. Build. Mater.* **2009**, *23*, 3532–3536. [[CrossRef](#)]